Sensitivity studies for extraction of GEn from inclusive and semi-inclusive electron scattering on polarized 3He

doi: 10.1103/PhysRevC.65.044002

Sensitivity studies for extraction of G_E^n from inclusive and semi-inclusive electron scattering on polarized ^{3}He

J. Golak,[1,2] W. Glöckle,[1] H. Kamada,[3] H. Witała,[2] R. Skibiński,[2] and A. Nogga[4]
[1]*Institut für Theoretische Physik II, Ruhr Universität Bochum, D-44780 Bochum, Germany*
[2]*Institute of Physics, Jagiellonian University, PL-30059 Cracow, Poland*
[3]*Department of Physics, Faculty of Engineering, Kyushu Institute of Technology, 1-1 Sensuicho, Tobata, Kitakyushu 804-8550, Japan*
[4]*Department of Physics, University of Arizona, Tucson, Arizona 85721*
(Received 5 November 2001; published 19 March 2002)

The processes $\overrightarrow{^3\mathrm{He}}(\vec{e},e')$ and $\overrightarrow{^3\mathrm{He}}(\vec{e},e'n)$ are theoretically analyzed with the aim to search for sensitivities in the electric form factor of the neutron, G_E^n. Faddeev calculations based on the high-precision NN force AV18 and using consistent mesonic exchange currents are employed. While the inclusive process is too insensitive, the semiexclusive one appears promising.

DOI: 10.1103/PhysRevC.65.044002 PACS number(s): 21.45.+v, 24.70.+s, 25.10.+s, 25.40.Lw

I. INTRODUCTION

The experimental knowledge of electromagnetic form factors of the neutron is of basic interest for testing model or finally QCD based predictions. Quite intensive experimental efforts are planned [1] and have been undertaken to extract these form factors from electron scattering on the deuteron [2–5] and ^{3}He [6–9]. In Ref. [8] the magnetic neutron form factor G_M^n has been extracted from the process $\overrightarrow{^3\mathrm{He}}(\vec{e},e')$ at $q^2=0.1$ and 0.2 $(\mathrm{GeV}/c)^2$. The analysis of the data relied on precise solutions of the $3N$ Faddeev equations for ^{3}He and the $3N$ continuum, thereby using modern nuclear forces and consistent mesonic exchange currents (MEC's). The resulting values for G_M^n agreed perfectly with results extracted from the cross section ratio $d(e,e'n)/d(e,e'p)$ [3]. The experimental data for higher q^2 values have not yet been analyzed in the same framework because it has to be expected that relativistic corrections will play a significant role and the theoretical framework for that extension has not yet been settled enough to be reliably applicable. This is an important challenge and task for theory.

In the case of G_E^n the experiments [6,7] for the process $\overrightarrow{^3\mathrm{He}}(\vec{e},e'n)$ had the aim to extract the electric form factor of the neutron. The analysis, however, leaves more questions of reliability open than in the case of G_M^n. Around $q^2=0.35$ $(\mathrm{GeV}/c)^2$ a first result [6] was based on the simple assumption that polarized ^{3}He can be considered to be a polarized neutron. This was later corrected by a Faddeev calculation [9], however, without taking MEC's into account. Also, relativistic effects in that Faddeev calculation were not included, though they might be not negligible. The corrections induced by final state interactions (FSI) turned out to be substantial and moved the original value towards the region of G_E^n values found in the experiments based on a deuteron target [4,5]. The theoretical analysis of that experiment [9] was also aggravated by a heavy averaging over the experimental conditions. At an even higher q^2 value of $q^2=0.67$ $(\mathrm{GeV}/c)^2$ the same process was again used under the same assumption of replacing $\overrightarrow{^3\mathrm{He}}$ by a polarized neutron to extract a value of G_E^n [7]. Corrections coming from a full ^{3}He wave function and rescattering processes have not yet been estimated.

In such a situation it is of interest to theoretically investigate electron induced ^{3}He observables with respect to their sensitivity to G_E^n. The ideas [10] for choosing certain observables are based on plane wave impulse approximation and the fact that the polarization of ^{3}He is carried with about 90% by the polarized neutron. Thus it is well known (see, for instance, Ref. [11]) that under neglection of FSI and keeping only the principal S state an asymmetry based on scattering of a polarized electron on a ^{3}He target polarized perpendicular to the (virtual) photon direction is proportional to $G_E^n G_M^n$. In Ref. [12] inclusive scattering has been investigated under the assumption of PWIA but keeping a full ^{3}He wave function with the pessimistic result that the proton contribution overwhelms the signature of G_E^n. Note that PWIA in Ref. [12] includes the action of the NN t-operator within the spectator pair of nucleons and thus takes FSI partly into account. The question remains: What happens under the full dynamics? Based on the same simple picture one can form a ratio of two asymmetries, one with the ^{3}He spin perpendicular and one parallel to the photon direction. That ratio will be proportional to G_E^n/G_M^n. In order to focus more on the neutron one uses the $\overrightarrow{^3\mathrm{He}}(\vec{e},e'n)$ reaction and measures the knocked out neutron in coincidence with the scattered electron. Again the important question arises: Will sensitivity to G_E^n remain when the full dynamics is taken into account?

We investigate these questions using full fledged Faddeev calculations and modern nuclear forces and including MEC's as well. We restrict ourselves to a strictly nonrelativistic treatment even if we go into higher q^2 ranges, where relativity should and will play a role. At least we can get insight into the importance or decrease of importance of FSI.

The paper is organized as follows. In Sec. II we briefly review the theoretical framework. Our results for inclusive scattering and for the semiexclusive processes are shown in Sec. III. We summarize in Sec. IV and end with an outlook.

II. THEORETICAL FRAMEWORK

The cross section for the process $\overrightarrow{^3\mathrm{He}}(\vec{e},e')$ is given as [13]

$$\frac{d^3\sigma}{d\hat{k}'dk_0'}=\sigma_{\rm Mott}\{v_L R^L+v_T R^T + h(v_{TL'}R^{TL'}+v_{T'}R^{T'})\}, \quad (1)$$

where k_0', $\hat{k}'$ are the energy and direction of the scattered electron, v_L, v_T, $v_{TL'}$, $v_{T'}$ are kinematical factors, R^L, R^T, $R^{TL'}$, $R^{T'}$ response functions, and h is the helicity of the initial electron. The asymmetry is defined as

$$A=\frac{\left.\frac{d^3\sigma}{d\hat{k}'dk_0'}\right|_{h=1}-\left.\frac{d^3\sigma}{d\hat{k}'dk_0'}\right|_{h=-1}}{\left.\frac{d^3\sigma}{d\hat{k}'dk_0'}\right|_{h=1}+\left.\frac{d^3\sigma}{d\hat{k}'dk_0'}\right|_{h=-1}}=-\frac{v_{T'}\tilde{R}^{T'}\cos\theta^\star+2v_{TL'}\tilde{R}^{TL'}\sin\theta^\star\cos\phi^\star}{v_L R^L+v_T R^T}, \quad (2)$$

where the dependence on $\theta^\star$ and $\phi^\star$ has been shown explicitly. These angles denote the direction of the ^{3}He spin in relation to the direction of the photon. (In contrast to Ref. [11] we modified slightly the definition of the $\tilde{R}$ responses.) In Ref. [11] it is shown that in PWIA and under the assumption of keeping only the principal S state of the ^{3}He wave function that asymmetry is given as

$$A^{\rm PWIA}=\frac{-\frac{q^2}{2m_N^2}\tan\frac{\Theta}{2}\left[\sqrt{\frac{q^2}{\vec{Q}^2}+\tan^2\frac{\Theta}{2}}(G_M^{(n)})^2\cos\theta^*+\frac{2m_N}{|\vec{Q}|}F_1^{(n)}G_M^{(n)}\cos\phi^*\sin\theta^*\right]}{(F_1^{(n)})^2+2(F_1^{(p)})^2-\frac{q^2}{4m_N^2}\left[(G_M^{(n)})^2+2(G_M^{(p)})^2+\alpha\frac{6m_N^2}{|\vec{Q}|^2}((F_1^{(n)})^2+2(F_1^{(p)})^2)\right]\left(1+2\tan^2\frac{\Theta}{2}\right)}. \quad (3)$$

(Note that in Ref. [11] PWIA has another meaning compared to Ref. [12]; we neglect all FSI.) There is a reminder of the ^{3}He wave function, the quantity α, which, however, is numerically insignificant [11]. We now replace F_1^n in the charge density operator by G_E^n. Because of the smallness of F_1^n the ''relativistic correction''

$$G_E^n=F_1^n-\frac{q^2}{4m_N^2}(G_M^n-F_1^n)\approx F_1^n-\frac{|\vec{Q}|^2}{4m_N^2}(G_M^n-F_1^n) \quad (4)$$

is mandatory. [Please note a misprint in Eq. (78) of Ref. [11]: the square bracket in the denominator should end not before but behind $\tan^2(\Theta/2)$.] Our notation for the photon momentum is $Q=(\omega,\vec{Q})$ and $-Q^2=q^2=\vec{Q}^2-\omega^2$. Regarding Eq. (3) we see that $\theta^*=0°$ (90°) emphasizes $(G_M^n)^2$ ($G_E^n G_M^n$). In the present investigation we shall study the dependence of $A_\perp\equiv A(\theta^*=90°,\phi^*=0°)$ on G_E^n including FSI and MEC's. We shall also provide insight into the contributions arising from photon absorption on the protons. This extends first studies carried through in Ref. [11], where only FSI effects were investigated.

The second process we are going to study is $\overrightarrow{^3\mathrm{He}}(\vec{e},e'n)$. The sixfold differential cross section is given as [13]

$$\frac{d^6\sigma}{d\hat{k}'dk_0'd\hat{p}_n dE_n}=\mathcal{C}\sigma_{\rm Mott}p_n\frac{pm_N^2}{2}\int d\hat{p}\{v_L R^L+v_T R^T+v_{TT}R^{TT}+v_{TL}R^{TL}+h(v_{TL'}R^{TL'}+v_{T'}R^{T'})\}, \quad (5)$$

where in addition to what has been said before $\hat{p}_n$, p_n, E_n, p, $\hat{p}$ denote the neutron direction, its momentum, its (nonrelativistic) kinetic energy, the magnitude of the relative momentum of the two undetected protons, and its direction. $\mathcal{C}=\frac{1}{2}$ for two undetected protons. Note that $\mathcal{C}=1$ for the $\overrightarrow{^3\mathrm{He}}(\vec{e},e'p)$ reaction.

Now the asymmetry defined in the same manner in relation to the electron helicities is given as

$$A=\frac{\int d\hat{p}(v_{T'}R^{T'}+v_{TL'}R^{TL'})}{\int d\hat{p}(v_L R^L+v_T R^T+v_{TT}R^{TT}+v_{TL}R^{TL})}. \quad (6)$$

We form the ratio $A_\perp/A_\parallel$, where $A_\perp(A_\parallel)$ refers to $\theta^*=90°$ (0°) and study its sensitivity to changes in G_E^n and FSI as well as MEC influences. It will also be of interest to see the proton contribution to that ratio, which is mostly caused by rescattering. The technical performance in momentum space and the necessarily involved partial wave decomposition has been described in Ref. [9] and references therein.

III. RESULTS

We first regard the process $\overrightarrow{^3\mathrm{He}}(\vec{e},e')$. Throughout we use the high precision NN force Argonne V18 potential (AV18) [14] together with π- and ρ-like MEC's [15] according to the Riska prescription [16]. As a reference model we take the Höhler parametrization for all electromagnetic form factors of the nucleons [17]. There are more recent param-

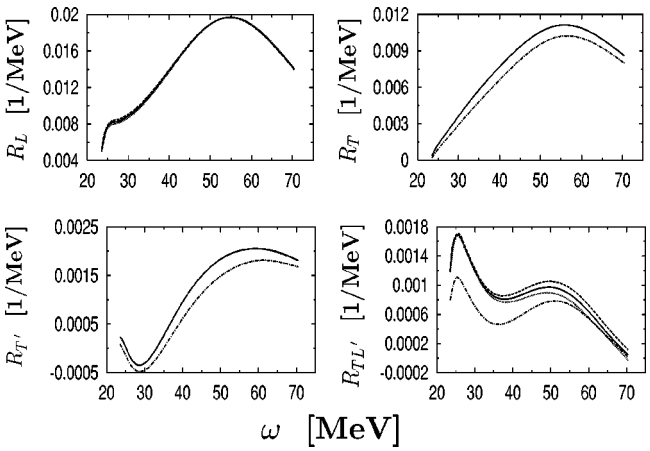

FIG. 1. R_L, R_T, $R_{T'}$, and $R_{TL'}$ for $q^2=0.1$ $(\mathrm{GeV}/c)^2$. Full (solid curves), FSI without MEC (dash-dotted curves), full with $1.6G_E^n$ (dashed curves), and with $0.4G_E^n$ (dotted curves).

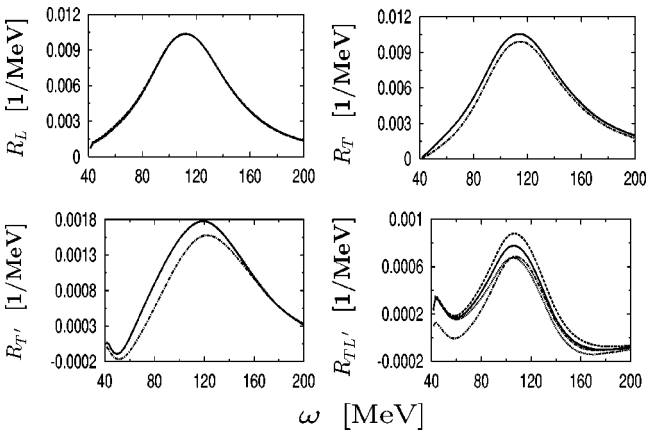

FIG. 2. The same as in Fig. 1 for $q^2=0.2$ $(\mathrm{GeV}/c)^2$.

etrizations, which are based on newer data, fulfill constraints of pQCD, etc. [18], and which, however, would not change the conclusions of our study. Besides the neglect of relativistic corrections, the knowledge of the MEC's might be a second concern about theoretical uncertainties. While the *NN* force chosen has been at least adjusted to the rich set of *NN* data, the choice of MEC's is not constrained in a corresponding manner. The ones we are using are, however, at least in harmony with the continuity equation. Also, one might expect that the best known π-like terms are the dominant ones. Nevertheless, in view of this situation we would like to show results without and with inclusion of MEC's. Thus one can see the magnitudes of the shifts caused by the MEC's alone. The calculations including FSI and MEC's will be denoted by ''full'' in the following. What we call the symmetrized plane wave approximation (PWIAS) does not include FSI nor MEC's but allows photon absorption on all three nucleons. This can also be expressed as photon absorption, say on nucleon 1, but then keeping fully antisymmetrized plane waves in the final state. We show in Figs. 1 and 2 the four response functions R_L, R_T, $R_{T'}$, and $R_{TL'}$ as a function of the energy transfer ω. The first (second) case shown in Fig. 1 (Fig. 2) corresponds roughly to $q^2=0.1$ (0.2) $(\mathrm{GeV}/c)^2$. More precisely, in the two cases we have chosen the initial electron energy to be 778 (1728) MeV and the electron scattering angle as $23.7(15.0)°$. There are always four curves: one is the reference curve with the G_E^n as given in Ref. [17] and full dynamics and another one with FSI but without MEC's. The two other curves are of full type but G_E^n is multiplied by 1.6 and 0.4, respectively. R_L is not affected by MEC's since we do not include two-body densities. Its dependence on G_E^n is marginal, since R_L is dominated by the proton. Besides into the density operator, G_E^n also enters into the MEC's, but there only as a difference to the proton form factor. Consequently changes of G_E^n hardly affect R_T and $R_{T'}$. Still the both response functions are visibly changed by MEC's. $R_{TL'}$ is the only response function of interest in searching for G_E^n sensitivities. There we see quite a strong effect of MEC's, which might introduce a certain theoretical uncertainty. For the MEC's chosen the $\pm 60\%$ changes in G_E^n lead to about $\pm 8\%$ changes in $R_{TL'}$ in its quasielastic peak region around $\omega=50$ MeV. This is for $q^2=0.1$ $(\mathrm{GeV}/c)^2$.

For $q^2=0.2$ $(\mathrm{GeV}/c)^2$ those changes are larger. They amount to $\pm 13\%$ in the quasielastic peak region around $\omega=100$ MeV. This is highly insufficient to serve as a signature for G_E^n. The reason for these small changes lies in the strong proton contribution as already shown in Ref. [12], based, however, on a PWIA calculation. This is now confirmed using the full dynamics.

We performed one calculation for each q^2 in the peak

TABLE I. Response functions for inclusive scattering and for two q^2 values at ω values in the peak region. The full calculation is compared to calculations without absorption of the photon on the proton. All responses are given in units of 1/MeV.

	$q^2=0.1$ $(\mathrm{GeV}/c)^2$, $\omega=50$ MeV			
	R_L	R_T	$R_{T'}$	$R_{TL'}$
Full	1.91×10^{-2}	1.07×10^{-2}	1.86×10^{-3}	9.68×10^{-4}
Full (no proton)	1.19×10^{-5}	1.38×10^{-3}	1.35×10^{-3}	1.24×10^{-4}
	$q^2=0.2$ $(\mathrm{GeV}/c)^2$, $\omega=110$ MeV			
	R_L	R_T	$R_{T'}$	$R_{TL'}$
Full	1.04×10^{-2}	1.06×10^{-2}	1.72×10^{-3}	7.82×10^{-4}
Full (no proton)	1.81×10^{-5}	1.47×10^{-3}	1.42×10^{-3}	1.57×10^{-4}

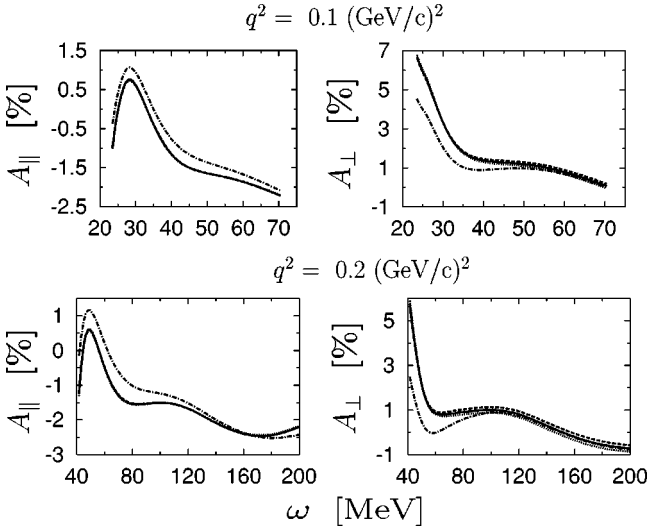

FIG. 3. $A_\parallel$ and $A_\perp$ for $q^2=0.11$ and 10.2 $(\mathrm{GeV}/c)^2$. Curves as in Fig. 1.

region dropping all proton electromagnetic form factors. The results are shown in Table I. We see that R_L is totally dominated by photon absorption on the proton. The reductions for R_T by switching off the proton contribution are about 87%, while they are much less for $R_{T'}$, namely about 27%. Now in case of $R_{TL'}$ one has reductions of 87% and 80% at $q^2=0.1$ and 0.2 $(\mathrm{GeV}/c)^2$, which explains the insufficient sensitivity against changes in G_E^n at these q^2 values. We refrained from investigating higher q^2 values because missing relativistic effects might change the results. There is no need to compare with PWIAS calculations, since they are known [19] to be insufficient.

Since for those changes of G_E^n the shifts in R_L and R_T are negligible, the changes in the asymmetry $A_\perp$ reflect directly the changes in $R_{TL'}$. This is shown in Fig. 3, which for the sake of completeness also includes $A_\parallel$. We see first of all the strong shifts caused by the MEC's. Then around $\omega=50$ (100) MeV for $q^2=0.1(0.2)(\mathrm{GeV}/c)^2$ small modifications of $A_\perp$ of about $\pm 8(13)\%$ are seen caused by the $\pm 60\%$ variations

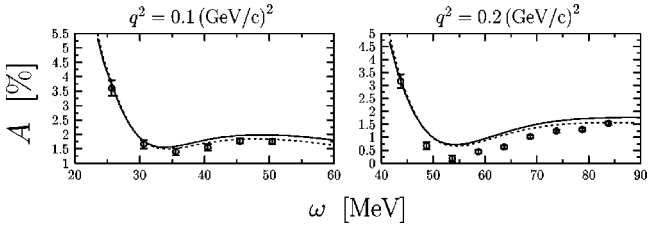

FIG. 4. Comparison of data (Ref. [21]) at $q^2=0.1$ and 0.2 $(\mathrm{GeV}/c)^2$ with two full point geometry calculations using F_1^n (dashed curves) and G_E^n (solid curves), respectively.

in G_E^n. The strong proton contribution explains the insufficient sensitivity against G_E^n.

The measurements of both asymmetries are nevertheless of great importance. $A_\parallel$ has been used recently [8] to extract G_M^n, as mentioned in the introduction. Pioneering measurements on the asymmetry $A_\perp$ have been performed in Ref. [20]. They have been analyzed in Ref. [11], however without MEC's and using F_1^n instead of G_E^n in the single nucleon density operator. The agreement with those data was quite good. More recently the asymmetry given in Eq. (2) was measured around $\theta^\star=130$ to 140° [21]. We analyzed the data with calculations of the full type. The agreement was quite good at $q^2=0.1$ $(\mathrm{GeV}/c)^2$ but an overshooting of the theory was observed for $q^2=0.2$ $(\mathrm{GeV}/c)^2$. It has to be remarked that in those calculations still F_1^n has been used in the single nucleon density operator. Despite the fact that a strong proton contribution is present, the changes by going from F_1^n to G_E^n are noticeable. We document that in Fig. 4 by comparing the data at $q^2=0.1$ and 0.2 $(\mathrm{GeV}/c)^2$ [21] with two full calculations using F_1^n and G_E^n, respectively. Using G_E^n leads to a slight deterioration in comparison to the F_1^n result.

Let us now move on to the process $\overrightarrow{^3\mathrm{He}}(\vec{e},e'n)$ and check whether it is more sensitive to G_E^n. As emphasized before our present strictly nonrelativistic framework does not allow reliable predictions at high q^2 values, say above $q^2=0.2$ $(\mathrm{GeV}/c)^2$. Nevertheless we shall now exhibit results beyond that with the only aim to describe possible trends for

TABLE II. Kinematical quantities for quasifree scattering conditions studied in the present work. The electron beam energy was fixed to 1 GeV. Subscripts ''nrl'' and ''rel'' refer to the nonrelativistic and relativistic treatment of kinematics.

q^2 $[(\mathrm{GeV}/c)^2]$	ω_{nrl} (MeV)	Q_{nrl} (MeV/c)	ω_{rel} (MeV)	Q_{rel} (MeV/c)	$E_{\mathrm{nrl}}^{\mathrm{c.m.}}$ (MeV)	$E_{\mathrm{rel}}^{\mathrm{c.m.}}$ MeV
0.05	27.0	225.2	26.6	225.2	12.5	12.2
0.10	54.8	320.9	53.2	320.7	31.1	29.7
0.15	83.6	396.2	79.9	395.4	50.3	47.2
0.20	113.3	461.6	106.5	459.7	70.1	64.5
0.25	144.2	520.4	133.1	517.4	90.6	81.8
0.30	176.3	575.4	159.7	570.5	112.0	98.9
0.35	209.8	627.7	186.4	620.3	134.4	116.0
0.40	244.9	678.2	213.0	667.4	157.8	132.9
0.45	281.9	727.7	239.6	712.3	182.5	149.7
0.50	321.1	776.6	266.2	755.6	208.6	166.5

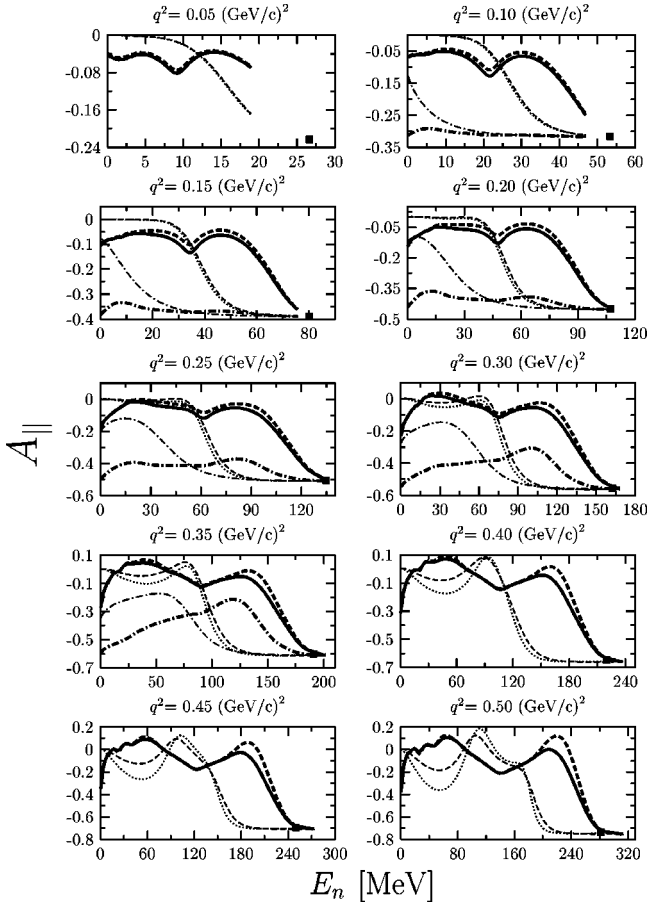

FIG. 5. $A_\parallel$ as a function of the neutron energy E_n for different q^2 values. Full (solid), FSI without MEC (dashed, thick line), full without proton contribution (dash-dotted, thick line), PWIAS (dashed, thin line), PWIAS with the relativistic single nucleon current (dotted) and PWIAS without proton contribution (dash-dotted, thin line); pure neutron result (filled square). The dashed-dotted lines occur only for q^2 from 0.1 to 0.35 $(\mathrm{GeV}/c)^2$.

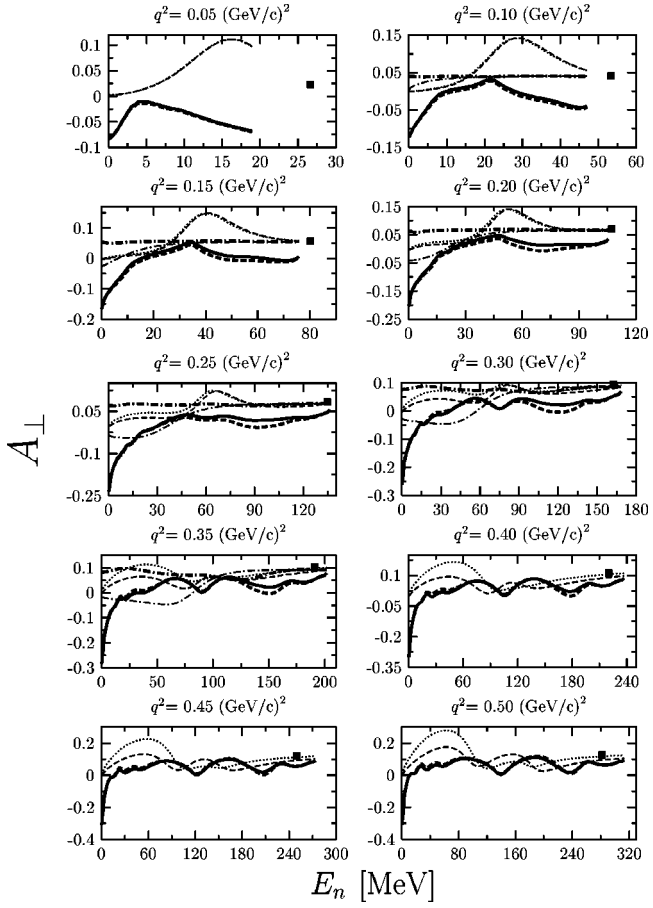

FIG. 6. $A_\perp$ as a function of the neutron energy E_n for different q^2 values. Curves and the symbol as in Fig. 5.

the significance of FSI and MEC's. We cannot exclude that these results might change in the future to an unknown extent, when relativity will be correctly included.

With respect to extracting neutron information, it appears optimal to choose a breakup configuration where the neutron is knocked out in the direction of the photon. On top one can assume that the neutron receives the full photon momentum and moreover the photon energy equals the final neutron energy. This is often called the quasifree scattering condition. We choose ten different q^2 values as shown in Table II. The related photon energy ω, its three momentum $|\vec{Q}|$, and the c.m. energy of the final three nucleons $E^{\mathrm{c.m.}}$ (all evaluated nonrelativistically) are also given. For the sake of orientation, corresponding relativistic values are included as well. The comparison of these parameters shows already that at the high q^2 values relativity cannot be neglected.

In the following figures, Figs. 5–7, we compare first of all results for PWIAS, full, and calculations with FSI but without MEC's. On top we add the result for the scattering on a free neutron at rest. This is treated fully relativistically and will be referred to in the figures as the pure neutron result. Though we concentrate in this paper on kinematical regions which are optimal to extract neutron information, we would also like to use the occasion to point to other regions in phase space where one can study the reaction mechanism and thus nuclear dynamics. Therefore we not only show the high energy region of the knocked out neutron but the ob-

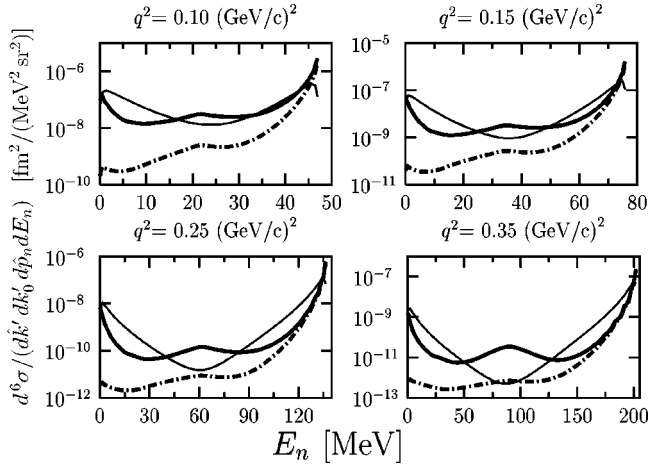

FIG. 7. The sixfold differential cross section as a function of the neutron energy E_n for different q^2 values. Full (solid, thick line), PWIAS (solid, thin line), and full without proton contribution (dash-dotted).

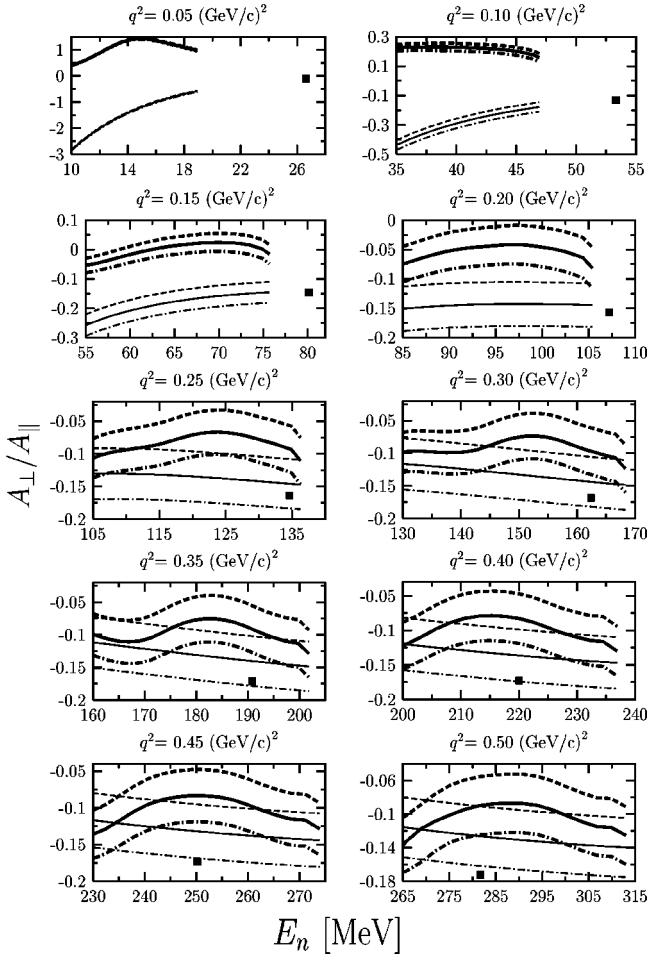

FIG. 8. The ratio $A_\perp/A_\parallel$ as a function of the neutron energy E_n for different q^2 values. The thick lines are full with $1.0G_E^n$ (solid), full with $0.75G_E^n$ (dashed), and full with $1.25G_E^n$ (dash-dotted). The thin lines are the corresponding cases for PWIAS. Filled square is the pure neutron result.

servables for all neutron energies, where for the lower ones the proton contribution in the photon absorption is very substantial. This is clearly exhibited by displaying also predictions where all electromagnetic proton form factors are set to zero and thus the photon is absorbed only on the neutron.

Finally in PWIAS, which is based on a single nucleon current, we show also results where the nonrelativistic single nucleon current is replaced by the fully relativistic one. This idea has been put forward before by Jeschonnek and Donnelly [22]. Our way to represent that relativistic current which is ideal for a straightforward extension of the partial wave representation we use up to now is given in the Appendix.

We show the observables $A_\parallel = A(\theta^\star = 0°)$ in Fig. 5 and $A_\perp = A(\theta^\star = 90°)$ in Fig. 6. Furthermore as guidance for experiments we also provide the sixfold differential cross section in Fig. 7.

Lets start with $A_\parallel$. Roughly speaking the picture is the same for all q^2 values with the exception of the lowest one. The full result rises quickly from the highest neutron energy E_n and then with some small oscillations remains essentially

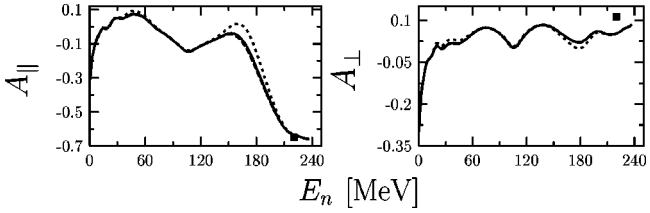

FIG. 9. $A_\parallel$ and $A_\perp$ as a function of the neutron energy E_n for $q^2 = 0.4$ (GeV/c)^2. FSI without MEC (dotted), full with π-like MEC only (dashed), and full with π- and ρ-like MEC (solid).

flat towards smaller energies. At the higher end of the neutron energy it is close to the pure neutron value for $q^2 = 0.2$ (GeV/c)^2 and higher momentum transfers. The effect of MEC is most pronounced at the first bump after the sharp rise. PWIAS is drastically different in the region of higher neutron energies, except at the very end, where all curves coincide. Thus FSI should be taken into account if, because of experimental reasons, some averaging over neutron energies is needed. The fully relativistic single nucleon current inserted into a PWIAS calculation has only a minor effect at the high neutron energies, but it changes the results at the lower ones above $q^2 = 0.3$ (GeV/c)^2 quite significantly. For some q^2 values we dropped artificially the proton contribution by switching off all electromagnetic proton form factors. This leads to a drastic change in PWIAS and the full calculation at all energies (except the very highest ones). The two smallest q^2 values are special, especially $q^2 = 0.05$ (GeV/c)^2, where the full calculation is far away from the pure neutron result.

In this paper we are mainly concerned with the G_E^n effects in $A_\perp$. Again we find that the rough overall behavior of the full result is similar for all q^2 values, except for the two lowest ones. At the high q^2 values oscillations develop as a function of the neutron energy and the effect of MEC's diminishes. In any case MEC effects are mild and disappear in the high energy region. But FSI remains important for all q^2 values, as is obvious by comparing to the PWIAS results. While the latter ones reach the pure neutron value at the high energy end the full curves stay always below that value. The effect of the relativistic single nucleon current is again strongly noticeable at $q^2 = 0.3$ (GeV/c)^2 and higher momentum transfers. The proton contribution is quite significant, as shown in some examples. At the two small q^2 values calculations without FSI would obviously be totally meaningless.

Figure 7 displays the sixfold differential cross section against the neutron energy for a few examples of q^2 values. We see a steep rise at the high neutron energies due to the $^1S_0$ t-matrix pole in the pp subsystem near zero subsystem energy. Since we did not include the Coulomb force the cross section values at the very end might change if that approximation can be avoided in the future. The cross section drops quickly by orders of magnitudes going to smaller E_n values. At the very low energies there is again a rise which is due to photon absorption on the protons, as also shown in the figures. At the very high energy end the proton contribution is dying out. It is also clear that in all cases PWIAS is highly insufficient.

Now we focus on the central issue, namely the sensitivity of $A_\perp$ and of $A_\perp/A_\parallel$ with respect to changes in G_E^n. Since the cross section drops rapidly with decreasing neutron energy and since only at high energies results of the $3N$ calculations can be used to extract neutron information, we present in Fig. 8 only a high neutron energy range. We show results for choosing G_E^n according to the fixed Höhler parametrization and to the values $1.25G_E^n$ and $0.75G_E^n$. Since $A_\parallel$ is not affected we display only $A_\perp/A_\parallel$ in Fig. 8. There are six curves, three for PWIAS and three for the full calculations. As already noticed in the results for $A_\perp$, we also see that FSI can never be neglected. If one regards, for instance, the range of about 20 MeV below the highest neutron energy, then for $q^2=0.35$ $(\mathrm{GeV}/c)^2$ and higher the full dynamics shifts the PWIAS results between 10% and 42%. This is comparable to the signature we are after, namely the changes of the full result by modifying G_E^n by $\pm 25\%$. At the highest neutron energy these changes start at $\pm 32\%$ for $q^2=0.25$ $(\mathrm{GeV}/c)^2$ and decrease slightly to $\pm 27\%$ at $q^2=0.50$ $(\mathrm{GeV}/c)^2$. Thus there are even enhancements in the changes of the ratio $A_\perp/A_\parallel$ against the ones in the variation of G_E^n. At the lower q^2 values PWIAS results would be totally meaningless. At $q^2=0.20$ $(\mathrm{GeV}/c)^2$ those changes in the ratio increase to $\pm 42\%$ and at $q^2=0.15$ $(\mathrm{GeV}/c)^2$ even to $\pm 204\%$. This drastic increase is, of course, caused by the smallness of that specific ratio. At the two smallest q^2 values the sensitivity drops rapidly, $\pm 17\%$ at $q^2=0.1$ $(\mathrm{GeV}/c)^2$ and $\pm 2\%$ at $q^2=0.05$ $(\mathrm{GeV}/c)^2$. The reason is the strong contribution of the proton as seen in Fig. 6. Clearly in all cases the pure neutron value is far off.

One can use the results presented in Fig. 8 to estimate roughly the error in the G_E^n extraction using only PWIAS. Regarding, for instance, the cases $q^2=0.3$ or 0.35 $(\mathrm{GeV}/c)^2$ and assuming that the experimental value for $A_\perp/A_\parallel$ measured near the high energy end would lie on the PWIAS curve (with G_E^n multiplied by the factor 1), then for the full calculation to agree with the experimental value one would have to increase the G_E^n value by 25% and more. Referred to the pure neutron value, this change would be even bigger. Of course, this estimate is very rough since the experimental conditions leading to averaging have to be taken into account and the magnitude of relativistic effects are basically unknown, but it clearly shows the need of full calculations for any analysis of such experiments.

Since the effects of MEC's are sometimes substantial, we investigated the separate contribution of the π-like MEC's. We found that it is by far the dominant one. This is illustrated in Fig. 9, for the example $q^2=0.4$ $(\mathrm{GeV}/c)^2$, which shows $A_\parallel$ and $A_\perp$. Three curves are displayed, FSI without MEC, full with π-like MEC only, and full with π- and ρ-like MEC, as in Figs. 5 and 6. Clearly the ρ-like MEC contribution is a small effect, and therefore our MEC estimate should be rather reliable.

IV. SUMMARY AND OUTLOOK

We performed Faddeev calculations for the processes $\overrightarrow{^3\mathrm{He}}(\vec{e},e')$ and $\overrightarrow{^3\mathrm{He}}(\vec{e},e'n)$ based on the NN force AV18 and consistent MEC's. The asymmetry $A_\perp$ in the inclusive process turned out to be not sensitive enough to G_E^n to allow its extraction. This is due to the strong proton contribution. Our studies were performed at $q^2=0.1$ and 0.2 $(\mathrm{GeV}/c)^2$, which, however, show a tendency for a decrease of the proton contribution with increasing four momentum transfer. Thus we cannot rule out that at higher q^2 values $A_\perp$ might be useful to extract G_E^n. Our nonrelativistic approach does not allow that realm to be entered into reliably.

The situation is, however, favorable in the neutron knockout process $\overrightarrow{^3\mathrm{He}}(\vec{e},e'n)$ to extract G_E^n information by measuring $A_\perp/A_\parallel$. In contrast to possible expectations FSI corrections are mandatory, as documented for several q^2 values up to the highest one which we studied, $q^2=0.5$ $(\mathrm{GeV}/c)^2$. Though we entered in the relativistic domain with purely nonrelativistic calculations it appears likely that the FSI effects found are fairly realistic. Therefore relying on $3N$ continuum calculations, whose quality has been tested beforehand in pure $3N$ scattering processes [23], one can extract from such measurements G_E^n information. There are, however, still theoretical uncertainties related to MEC's and, of course, relativistic effects.

As a first step into relativity we used the fully relativistic single nucleon current operator in a PWIAS calculation and found indeed quite significant changes, but fortunately not in the high energy end of the neutron spectrum, which is favorable for the G_E^n extraction.

Improvements in the theoretical framework in the near future are planned. $3N$ forces will be included, as it is standard by now in pure $3N$ scattering (see, for instance, Ref. [24]) and further types of MEC's. Of special interest thereby will be to guarantee consistency to the nuclear forces.

Besides working with standard potential models, the application of effective field theory concepts in the form of chiral perturbation theory appears to be very promising in the low momentum region. This has already started in two-, three- and four-nucleon systems including the coupling to the photon field. For a recent overview and references see Ref. [25].

ACKNOWLEDGMENTS

This work was supported by the Deutsche Forschungsgemeinschaft (J.G.) and by the Polish Committee for Scientific Research. One of us (W.G.) would like to thank the Foundation for Polish Science for the financial support during his stay in Cracow. The numerical calculations have been performed on the Cray T90 of the NIC in Jülich, Germany.

APPENDIX: IMPLEMENTATION OF THE RELATIVISTIC SINGLE NUCLEON CURRENT

In this appendix we show how the relativistic single nucleon current is used in our calculations, especially in the context of the $3N$ system. The relativistic single nucleon current operator has the well-known form

$$j^{\mu}(0)=e\sum_{ss'}\int d\vec{l}\int d\vec{l}'\,\sqrt{\frac{m}{l_0}}\sqrt{\frac{m}{l_0'}}\bar{u}(l's')[F_1\gamma^{\mu}+iF_2\sigma^{\mu\nu}(l'-l)_{\nu}]u(ls)b^{\dagger}(l's')b(ls), \tag{A1}$$

where $l_0\equiv\sqrt{m^2+\vec{l}^2}$, $l_0'\equiv\sqrt{m^2+\vec{l}'^2}$ (m is the nucleon mass), and $b^{\dagger}(l's')$ and $b(ls)$ are nucleon creation and annihilation operators. It can be rewritten as

$$\begin{aligned}j^{\mu}(0)&=e\sum_{ss'}\int d\vec{l}\int d\vec{l}'\,\sqrt{\frac{m}{l_0}}\sqrt{\frac{m}{l_0'}}\bar{u}(l's')[G_m\gamma^{\mu}-F_2(l+l')^{\mu}]u(ls)b^{\dagger}(l's')b(ls)\\&\equiv e\sum_{ss'}\int d\vec{l}\int d\vec{l}'\,\mathcal{X}^{\dagger}_{s'}N^{\mu}(l,l')\mathcal{X}_s b^{\dagger}(l's')b(ls).\end{aligned} \tag{A2}$$

The last form shows a four-component 2×2 matrix operator acting on Pauli spinors $\mathcal{X}_s$. With

$$A\equiv\sqrt{\frac{m}{l_0}}\sqrt{\frac{m}{l_0'}}\sqrt{\frac{l_0'+m}{2m}}\sqrt{\frac{l_0+m}{2m}}, \tag{A3}$$

the components $N^{\mu}(l,l')$ are written as

$$N^0=A\left\{[G_m-F_2(l+l')^0]+[G_m+F_2(l+l')^0]\frac{\vec{l}'\cdot\vec{l}}{(l_0+m)(l_0'+m)}\right\}+A[G_m+F_2(l+l')^0]\frac{i\vec{\sigma}\cdot(\vec{l}'\times\vec{l})}{(l_0+m)(l_0'+m)}, \tag{A4}$$

$$\begin{aligned}N^k=&-AF_2\left(1-\frac{\vec{l}'\cdot\vec{l}}{(l_0+m)(l_0'+m)}\right)(l+l')^k+AG_m\left(\frac{l^k}{l_0+m}+\frac{l'^k}{l_0'+m}\right)\\&+AF_2\frac{(l+l')^k}{(l_0+m)(l_0'+m)}i\vec{\sigma}\cdot(\vec{l}'\times\vec{l})+AG_m\left[\frac{1}{(l_0+m)}i(\vec{l}\times\vec{\sigma})^k+\frac{1}{(l_0'+m)}i(\vec{\sigma}\times\vec{l}')^k\right].\end{aligned} \tag{A5}$$

Introducing standard Jacobi momenta $\vec{p},\vec{q}$ the current matrix element between initial φ and final φ' $3N$ states can be written as

$$\langle\varphi'\{M'\}\vec{\mathcal{P}}'|j^{\mu}(0)|\varphi M\vec{\mathcal{P}}\rangle=3\int d\vec{p}\int d\vec{q}\langle\varphi'\{M'\}|\vec{p},\vec{q}\rangle N^{\mu}(l',l)\left\langle\vec{p},\vec{q}+\frac{2}{3}\vec{\mathcal{P}}-\frac{2}{3}\vec{\mathcal{P}}'\middle|\varphi M\right\rangle, \tag{A6}$$

where $\vec{l}'\equiv\vec{q}+\frac{1}{3}\vec{\mathcal{P}}'$, $\vec{l}\equiv\vec{q}+\vec{\mathcal{P}}-\frac{2}{3}\vec{\mathcal{P}}'$. $\vec{\mathcal{P}}$ and $\vec{\mathcal{P}}'$ are the initial and final total $3N$ momenta, respectively.

We choose the laboratory frame ($\vec{\mathcal{P}}=\vec{0}$) and denote $\vec{Q}=\vec{\mathcal{P}}'-\vec{\mathcal{P}}=\vec{\mathcal{P}}'$. Furthermore because of current conservation we can restrict ourselves only to transverse components of N^k, and choose the spherical components N_{τ}, $\tau=\pm1$. Then expressions appearing in Eqs. (A4) and (A5) can be evaluated as

$$\vec{l}'\cdot\vec{l}=q^2-\frac{1}{3}\vec{q}\cdot\vec{Q}-\frac{2}{9}Q^2,\quad \vec{l}'\times\vec{l}=\vec{Q}\times\vec{q},\quad l_{\tau}=l_{\tau}'=q_{\tau},\quad (\vec{\sigma}\times\vec{l}')_{\tau}=(\vec{\sigma}\times\vec{q})_{\tau}+\frac{1}{3}(\vec{\sigma}\times\vec{Q})_{\tau},$$

$$(\vec{\sigma}\times\vec{l})_{\tau}=-(\vec{\sigma}\times\vec{q})_{\tau}+\frac{2}{3}(\vec{\sigma}\times\vec{Q})_{\tau}, \tag{A7}$$

and one can group some terms in Eq. (A5) together. One ends up with

$$\begin{aligned}N_{\tau}=&A\left\{G_m\left(\frac{1}{l_0+m}+\frac{1}{l_0'+m}\right)-2F_2\left(1-\frac{\vec{l}'\cdot\vec{l}}{(l_0+m)(l_0'+m)}\right)\right\}q_{\tau}+AG_m\left(\frac{\frac{2}{3}}{(l_0+m)}+\frac{\frac{1}{3}}{(l_0'+m)}\right)i(\vec{\sigma}\times\vec{Q})_{\tau}\\&+AG_m\left(\frac{1}{(l_0+m)}-\frac{1}{(l_0'+m)}\right)i(\vec{q}\times\vec{\sigma})_{\tau}+A2F_2\frac{q_{\tau}}{(l_0+m)(l_0'+m)}i\vec{\sigma}\cdot(\vec{Q}\times\vec{q}).\end{aligned} \tag{A8}$$

In the nonrelativistic limit only the correspondingly reduced first two terms in Eq. (A8) remain; the first one is the

convection current, the second is the spin current. The partial wave decomposition can be carried through by straightforward extension of the forms given in Ref. [19]. As a subtle point we mention that the arguments of the electromagnetic form factors are not the four-momentum squared of the photon but $(l_0-l_0')^2-(\vec{l}-\vec{l}\,')^2$. This is required in a Hamiltonian formalism where only the three-momenta are conserved at the vertices and not the four-momenta as in a manifest covariant formalism.

[1] R. Alarcon, Prog. Part. Nucl. Phys. **44**, 253 (2000).

[2] C. W. de Jager, in *Bates 25: Celebrating 25 Years of Beam to Experiment*, edited by T. W. Donnelly and W. Turchinetz, AIP Conf. Proc. No. 520 (AIP, Woodbury, NY, 2000), p. 225.

[3] H. Anklin *et al.*, Phys. Lett. B **428**, 248 (1998).

[4] I. Passchier *et al.*, Phys. Rev. Lett. **82**, 4988 (1999).

[5] C. Herberg *et al.*, Eur. Phys. J. A **5**, 131 (1999).

[6] J. Becker *et al.*, Eur. Phys. J. A **6**, 329 (1999).

[7] D. Rohe *et al.*, Phys. Rev. Lett. **83**, 4257 (1999).

[8] W. Xu *et al.*, Phys. Rev. Lett. **85**, 2900 (2000).

[9] J. Golak, G. Ziemer, H. Kamada, H. Witała, and W. Glöckle, Phys. Rev. C **51**, 034006 (2001).

[10] B. Blankleider and R.M. Woloshyn, Phys. Rev. C **29**, 538 (1984).

[11] S. Ishikawa, J. Golak, H. Witała, H. Kamada, W. Glöckle, and D. Hüber, Phys. Rev. C **57**, 39 (1998).

[12] R.-W. Schulze and P.U. Sauer, Phys. Rev. C **48**, 38 (1993).

[13] T.W. Donnelly and A.S. Raskin, Ann. Phys. (N.Y.) **169**, 247 (1986).

[14] R.B. Wiringa, V.G.J. Stoks, and R. Schiavilla, Phys. Rev. C **51**, 38 (1995).

[15] V.V. Kotlyar, H. Kamada, J. Golak, and W. Glöckle, Few-Body Syst. **28**, 35 (2000).

[16] D.O. Riska, Phys. Scr. **31**, 107 (1985); **31**, 471 (1985).

[17] G. Höhler, E. Pietarinen, I. Sabba-Stefanescu, F. Borkowski, G.G. Simon, V.H. Walther, and R.D. Wendling, Nucl. Phys. **B114**, 505 (1976).

[18] P. Mergell, Ulf-G. Meißner, and D. Drechsel, Nucl. Phys. **A596**, 367 (1996); H.-W. Hammer, Ulf-G. Meißner, and D. Drechsel, Phys. Lett. B **385**, 343 (1996).

[19] J. Golak *et al.*, Phys. Rev. C **52**, 1216 (1995).

[20] J.-O. Hansen *et al.*, Phys. Rev. Lett. **74**, 654 (1995); C.E. Jones *et al.*, Phys. Rev. C **52**, 1520 (1995).

[21] F. Xiong *et al.*, Phys. Rev. Lett. **87**, 242501 (2001).

[22] S. Jeschonnek and T.W. Donnelly, Phys. Rev. C **57**, 2438 (1998).

[23] W. Glöckle, H. Witała, D. Hüber, H. Kamada, and J. Golak, Phys. Rep. **274**, 107 (1996).

[24] H. Witała *et al.*, Phys. Rev. C **63**, 024007 (2001).

[25] E. Epelbaum, U.-G. Meißner, W. Glöckle, C. Elster, H. Kamada, A. Nogga, and H. Witała, in *Mesons and Light Nuclei: 8th Conference*, Prague, Czech Republic, 2001, edited by J. Adam and P. Bydzovský, and J. Mares, AIP Conf. Proc. No. 603 (AIP, Melville, NY, 2001), p. 17.